Engineering Failure Analysis 91 (2018) 58–71

Contents lists available at ScienceDirect

Engineering Failure Analysis

journal homepage: www.elsevier.com/locate/engfailanal

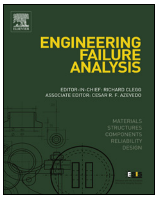

The effect of decarburized layer on rolling contact fatigue of rail materials under dry-wet conditions

X.J. Zhao, H.Y. Wang, J. Guo, Q.Y. Liu, G.T. Zhao, W.J. Wang*

Tribology Research Institute, State Key Laboratory of Traction Power, Southwest Jiaotong University, Chengdu 610031, China

ARTICLE INFO

Keywords:
Rail material
Decarburized layer
Rolling contact fatigue
Water lubrication
Crack

ABSTRACT

Decarburization means carbon in rail material lost in the hot rolled process. It changes the microstructure of rail materials and will influence their rolling contact fatigue (RCF) characteristic. The objective of this study is to explore the effect of decarburized layer on rolling contact fatigue and propagation mechanism of crack under the wet condition using a rolling-sliding wear testing machine. The results show that the crack growth rate on the decarburized rail roller is over 4 times than that on the non-decarburized rail. Small pitting presents on the non-decarburized rail roller, which is dominated by transgranular crack. While, long mouth surface crack dominates on the decarburized rail roller and the cracks mainly grow along the ferrite line or the grain boundary. With the cycles increasing, the surface cracks of decarburized rail roller gradually break and forms spalling damage, eventually expands to bulk spalling. Meanwhile, the crack growth mechanism changes back to the transgranular propagation and propagates in depth with a large angle when the decarburization is worn off.

1. Introduction

It is well known that the damage of the wheel and rail materials emerges due to cyclic rolling contact between the wheel tread and rail head, which has significant effects on service life of wheel/rail system. Damage such as rail corrugation [1], squat [2] and side wear caused by heavy load [3] may pose a threat to the security of railway. Therefore, by means of various experimental and numerical methods, a number of work have been carried out to explore how do the factors such as rail joint [4], plastic deformation [5], slip ratio [6], ambient temperature [7] and surface corrosion [8] affect the wear damage and RCF of the rail. Taizo [9] found that the fatigue strength of the rail by RCF tests decreasing with the increase in the slip ratio. Nejad [10] pointed that the fatigue life declines with an increase in stress field in wheel-rail contact zone. Moreover, the "third body" between the wheel and rail also influences fatigue life of rail. Hardwick [11] found that over the same slip range the water and grease contact exhibit distinct wear regimes and the damage mechanism according to the wear rate were plotted against $T\gamma/A$. Fletcher [12] presented that there could be a high growth rate for cracks containing pressurised fluid. Lewis [13] et al. assessed the wear rate, traction coefficient, and retentivity using two series of tests with ten current greases.

The microstructure is one of important factors influencing the RCF characteristics of rail materials. Su [14] found that low carbon bainitic rail has a weaker RCF resistance than pearlitic rail. As it is known, rail is manufactured by being cast continuously into bloom steel and hot rolled to the desired profile. The hot rolling process requires the bloom steel to be reheated to the temperature of 1200 °C. So, the decarburization may emerge on the rail surface due to the fact that the oxidization of carbon is faster than that of iron [15]. Furthermore, the carbon content of decarburized rail declines and the RCF resistance needs to be explored. It was concluded by

---

* Corresponding author.
E-mail address: wwj527@swjtu.cn (W.J. Wang).

https://doi.org/10.1016/j.engfailanal.2018.04.026
Received 20 December 2017; Received in revised form 5 April 2018; Accepted 11 April 2018

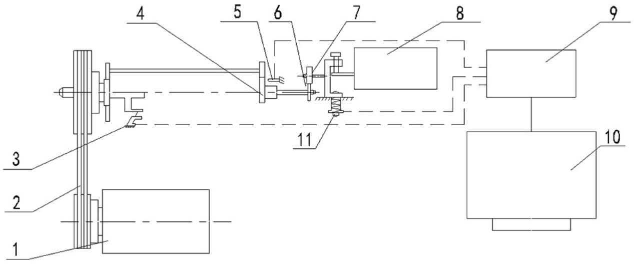

1. DC motor; 2. Drive belt; 3. Torque sensor; 4. Drive shaft gears; 5. Photosensor; 6. Lower roller; 7. Upper roller; 8. Driven shaft gears; 9. Controller; 10. Computer; 11. Load sensor

Fig. 1. Schematic diagram of the machine.

Boulanger [16] that the decarburized layer seldom affects RCF resistance of SNCF rails. However, Rottauser [17] found that the initiation of RCF cracks on grade 260 rail with 0.1 mm decarburization is delayed compared to that with none. Carroll [15] carried out many experiments to study on the effect of decarburized rail on its wear performance and crack growth mechanism. He illustrated the relationship of maximum sheer stress and crack propagation and pointed that the RCF is dominated by the applied stress system and influenced by microstructure of the sample, it was also concluded that the crack does not propagate through the easiest microstructural path but instead propagates through the pearlite with occasional meanders into the ferrite. Moreover, it is clearly regulated by British Standards Institute that no closed ferrite network shall be observed below 0.5 mm depth measured anywhere on the rail head surface [18].

In the previous experiments carried out by our group [19], the wear behaviors of rail roller with different depth of decarburization were investigated and the critical value of decarburization were also given, but how does the crack growth mechanism change when the decarburization gradually worn off is still a question, especially when the decarburization completely worn off, whether the crack is still critical to rail material. Therefore, in this study, the rail roller with the same decarburization under different cycles were carried out using a rolling-sliding wear testing machine. In particular, the crack growth mechanism at different wear phase were explored in details using various micro-examinations.

2. Experimental details

2.1. Experimental machine

All experiments were carried out using a rolling-sliding wear testing machine composed of a wheel specimen (lower roller) and a rail specimen (upper roller) [20]. Two rollers are driven and controlled by a DC motor. Two rollers are powered and controlled by a DC motor through the transmission gears (Fig. 1). The transmission gears are changeable to achieve a rolling-sliding motion (slippage) between the wheel/rail rollers. The upper specimen is fixed in a swinging bracket where a normal force (from 0 to 2000 N) can be applied and adjusted by a compressed spring, the vertical force is recorded by the force sensor fixed on the spring. A revolution counter is assembled on the drive shaft to measure the cycles of the lower specimen. The tangential and normal forces in the wheel/rail interface are automatically measured and recorded on the computer by means of the torque sensor [3] and load sensor [11] (measurement error: ± 5%), the instant friction coefficient can be calculate based on the signals captured by these sensors.

2.2. Microstructure of decarburized rail roller

In order to manufacture the artificial decarburized layer on the rail rollers, the rail specimens were reheated in the chamber furnace with air atmosphere at 1200 °C, and then keep them for 4 h, after that, air cooling to room temperature. Previous results [21] distinguish the decarburization from base material by connected ferrite network as Fig. 2 shows. In order to have a better observation of crack growth characters in different wear phase of decarburization, the decarburized area is further divided into two areas as Fig. 3a shows: complete decarburized area (about 0.5 mm in depth), partial decarburized area. The hardness of decarburized rail roller varies from surface to inner material, which also obviously distinguishes these areas (Fig. 3b). The complete decarburized area filled with ferrite network has the lowest hardness among these areas. The hardness in the partial decarburized area fluctuates from 200 to 250 $HV_{0.05}$ because the pearlite and ferrite mixed in this area. Lastly, the inner area with high hardness is defined as non-decarburized area.

2.3. Experimental parameters

The wheel and rail rollers were cut from the wheel tread and rail head, respectively. Their chemical compositions in weight percentage are given in Table 1. The normal force of 1100 N is applied to simulate the maximum contact pressure at about 890 MPa